Mechanical Response of Semi-Brittle Ceramics Subjected to Tension-Compression State. Part II: Description of Deformation Process

TOMASZ SADOWSKI*
Technische Universität München
Lehrstuhl A für Mechanik
80333 München, Arcisstrasse 21, Germany

ABSTRACT: Some numerical examples were presented to describe deformation process of semi-brittle polycrystalline ceramic materials, following paper [4]. The damage growth can be modelled as quasi-linear function of the stress state, what is easily applicable to solutions to many practical engineering problems.

1. INTRODUCTION

EXPERIMENTAL RESULTS PERFORMED on semi-brittle ceramics like MgO [1–3] lead to the conclusion that deformation process of this material passes through a sequence of phases. After purely elastic response, in some grain of the polycrystalline specimen a conjugate slip system is created (Figure 1). Under the external load dislocations pile up to the grain boundaries and produce microcracks. These microcracks spread along straight segments of grain boundaries creating so-called mesocracks. The final stage of deformation process, preceding the material failure, is kinking of mesocracks and their unconstrained development into macrocracks.

The theoretical description of all these phases was proposed in Reference [4] whereas this study will focus on the description of kinetics of considered process specifying crack shapes and their distribution within the unit cell. As the illustration of deformation process of this considered material uniaxial tension, pure shear and uniaxial compression were particularly analysed. Also limit surfaces for two-dimensional tension-compression were estimated.

*On leave from: Technical University of Lublin, Faculty of Civil and Sanitary Engineering, ul. Nadbystrzycka 40, 20–618 Lublin, Poland.

1056-7895/95/04 0293–26 $10.00/0

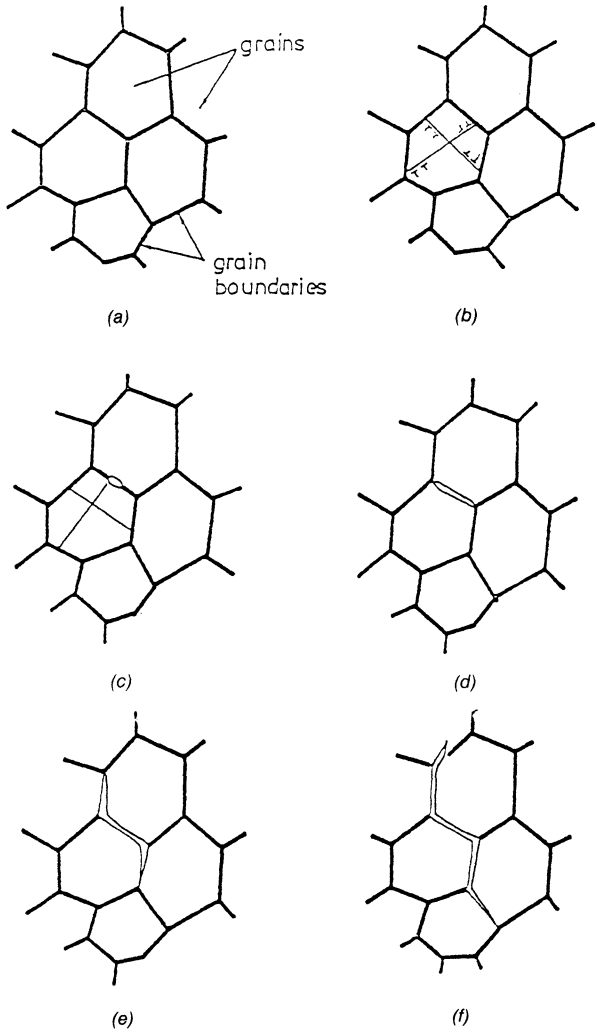

Figure 1. *Phases of MgO deformation process: (a) purely elastic; (b) slip lines (bands) development; (c) cracks initiation; (d) cracks development; (e) first kinking of cracks; (f) failure (secondary kinking)*

2. DEFORMATION PROCESS OF SEMI-BRITTLE POLYCRYSTALLINE CERAMICS

2.1. Constitutive Relations

According to Reference [4] the constitutive equations for continuous damage process can be expressed as a tensor function of two variables: the stress tensor $\underline{\sigma}$ and the second order damage tensor $\underline{\omega}$, i.e.

$$\underline{\epsilon} = \underline{\epsilon}(\underline{\sigma}, \underline{\omega}), \tag{1}$$

where $\underline{\epsilon}$ is the strain tensor. $\underline{\omega}$ has been assumed to be the only internal parameter.

In case of quasi-static deformation process, when the load increase is very slow, one can gain a direct relation between the tensors of damage and stress

$$\underline{\omega} = \underline{\omega}(\underline{\sigma}) \tag{2}$$

According to Equations (1) and (2) we have

$$\underline{\epsilon} = \underline{\underline{S}}(\underline{\sigma}, \underline{\omega}) : \underline{\sigma} \tag{3}$$

where

$$\underline{\underline{S}}(\underline{\sigma}, \underline{\omega}) = \underline{\underline{S}}^0 + \underline{\underline{S}}^*(\underline{\sigma}, \underline{\omega}) \tag{4}$$

In Equation (4) $\underline{\underline{S}}^0$ is the compliance tensor of the virgin material whereas $\underline{\underline{S}}^*$ is the compliance one which reflects all changes of internal structure within a unit cell of the polycrystalline material due to nucleation and propagation of all micro- and mesodefects (within grains or at grain boundaries). The particular discussion of the final form of $\underline{\underline{S}}^*$ related to respective kinds of defects was done in Reference [4]. With the assumption that flaws distribution is homogeneous and their density is dilute, the final form of $\underline{\underline{S}}^*$ can be obtained as superposition of influence of all defects. It results in the material response being highly nonlinear for loading, as will be presented in numerical examples.

Nonlinearity appears also during unloading process. It is due to effects of closing or backsliding mesocracks and kinks opening. The state of recoverable strains $\underline{\epsilon}^r$ will be estimated according to the following constitutive relations

$$\underline{\epsilon}^r = \underline{\underline{S}}^u(\underline{\sigma}, \underline{\omega}) : \underline{\sigma} \tag{5}$$

$\underline{\underline{S}}^u$ is the compliance tensor for unloading path. In general, its components differ from $\underline{\underline{S}}$ about the part connected with dislocation existence and the part describing modifications of the defect's shape.

2.2. Phenomenological Description of the Material Damage

Following References [4] and [5], one can simply propose the generalization of the phenomenological description of the damage state

$$\underline{\omega} \overset{def}{=} \frac{\Delta \underline{\epsilon}^r}{\underline{\epsilon}^r} \tag{6}$$

or in the index notation

$$\omega_{ij} \overset{def}{=} \frac{\Delta \epsilon^r_{ij}}{\epsilon^r_{ij}}$$

The tensor $\Delta \underline{\epsilon}^r$ in Equation (6) is a part of the total recoverable strain tensor $\underline{\epsilon}^r$, which reflects modification of the crack's shape within the unit cell during unloading:

$$\Delta \underline{\epsilon}^r = (\underline{\underline{S}}^u - \underline{\underline{S}}^0) : \underline{\sigma} \tag{7}$$

Taking into account Equations (5) and (7), relation (6) gains the final form

$$\underline{\omega} = \frac{(\underline{\underline{S}}^u - \underline{\underline{S}}^0) : \underline{\sigma}}{\underline{\underline{S}}^u : \underline{\sigma}} \tag{8}$$

2.3. Two-Dimensional Modelling

Numerical calculations will be performed for the two-dimensional loading process. With application of the Voigt's notation, relation (3) takes the form:

$$\epsilon_i = S_{ij}\sigma_j, \qquad i,j = 1,2,6 \tag{9}$$

In the present consideration we investigate the problem of damage development within the material, which is subjected to external loading characterized only by stress component σ_1 and σ_2. Additionally we assume that directions 1 and 2 do not change during whole process and the loading is so-called proportional:

$$\sigma_2 = q, \qquad \sigma_1 = kq \qquad \text{and} \qquad \sigma_{12} = 0 \tag{10}$$

In other words, we deal with the problem of damage propagation in the material under constant principal direction of macrostress. Other cases of loading will be described in References [6] and [7].

2.4. Deformation Process for Loading Path

The quasi-static deformation process of polycrystalline material is strictly characterized by the actual state of macrostress $\underline{\sigma}$. Passing the purely elastic phase, in some grains of the material dislocation sources activate to produce dislocations [Figure 1(b)]. They start to glide under shear stress τ, when τ is equal to the lattice resistance to easy slip τ_{so}:

$$\tau - \tau_{so} = 0 \tag{11}$$

Assuming that the first slip will occur in crystals having a slip plane at the angle of $\beta = 45°$, the fan of operative slip systems inside the unit cell is defined for the two-dimensional case, following Equation (11):

$$\sin 2\beta_s = \frac{2\tau_{so}}{(\sigma_2 - \sigma_1)} \tag{12}$$

Equation (12) has symmetrical roots with respect to 45°. The first two roots allow calulation of the number of grains with the two operative slip systems N_s according to:

$$N_s = \left(1 - \frac{4}{\pi}\beta_s\right)N \tag{13}$$

where N is the total number of grains within the unit cell.

Nucleated dislocations pile up to grain boundaries and create tensile stress in these parts of the material. In these conditions the Zener-Stroh crack can nucleate [Figure 1(c)], when the shear stress τ exceeds critical value τ_{co}:

$$\tau - \tau_{co} \geq 0 \tag{14}$$

τ_{co} can be estimated following [8, 9, and 5] as:

$$\tau_{co} = \left\{\frac{3\pi\gamma_{gb}G_0}{8(1 - \nu_0)d}\right\}^{1/2} + \tau_{so} \tag{15}$$

where γ_{gb} is the surface energy of grain boundaries and d is the pile-up length. G_0 and ν_0 are the Kirchhoff's modulus and Poisson's coefficient of the virgin material, respectively. Then the number of grains with slip bands potent enough to nucleate intergranular cracks is equal to

$$N_i = \left(1 - \frac{4}{\pi}\beta_c\right)N \tag{16}$$

where β_c is estimated from the criterion similar to Equation (12), but written for Equation (14). The number of mesocrack's nucleus was approximated in Reference [10].

$$N_c \cong 1.5\, N_i \tag{17}$$

In relation to the current state of macrostress $\underline{\sigma}$, a part of N_c nucleus develops into the straight segment of the grain boundary [Figure 1(d)], when the strain energy release criterion is satisfied [4]:

$$G(\phi) = 2\gamma_{gb} \tag{18}$$

These cracks influence the total material response to the applied load as:

- opened mesocracks

$$N_m^{(o)} = \frac{2(\phi_{c2}^{(o)} - \phi_{c1}^{(o)})}{\pi} N \tag{19}$$

- closed mesocracks

$$N_m^{(c)} = \frac{2(\phi_{c2}^{(c)} - \phi_{c1}^{(c)})}{\pi} N \tag{20}$$

Obviously, $N_m = N_m^{(o)} + N_m^{(c)}$ and $\phi_{c1} < \phi_c < \phi_{c2}$ denotes the fan of inclinations of the mesocracks N_m. The remaining microcracks $(N_c - N_m)$ stay closed (or suffer sliding) or opened and can spread for the higher level of loading. Their influence on the final constitutive relations is negligible.

Newly created mesocracks remain stable in a certain period of deformation process. They need additional increase of energy to overcome the energetic barrier connected with their deflection (toughening effect) and propagation along grain boundaries [Figure 1(e)]. The strain energy release criterion (18) takes, in the considered case, the more general form:

$$G(\phi,\theta) = \frac{1 - \nu_o}{E_o}(k_I^2 + k_{II}^2) = 2\gamma_{gb} \tag{21}$$

where k_I and k_{II} are the stress intensity factors along kinks direction (in points Q and Q' – see Figure 2) [4]:

$$k_I = -\frac{D}{2}\begin{Bmatrix} \tau_s \sin(\theta) \\ \sigma_6' \sin(\theta) + \sigma_2' \cos(\theta) \end{Bmatrix} \div [\pi(l + l^*)]^{1/2}$$

$$- (\pi l)^{1/2}\frac{1}{2}[\sigma_2 + \sigma_1 + (\sigma_1 - \sigma_2)\cos 2(\theta + \phi)] \tag{22}$$

$$k_{II} = \frac{D}{2}\begin{Bmatrix} \tau_s \cos(\theta) \\ \sigma_6' \cos(\theta) + \sigma_2' \sin(\theta) \end{Bmatrix} \div [\pi(l + l^*)]^{1/2}$$

$$- (\pi l)^{1/2}\frac{1}{2}[(\sigma_1 - \sigma_2) \sin 2(\theta + \phi)] \tag{23}$$

The upper expressions in the braces are related to closed mesocracks, whereas the lower expressions are related to opened ones. The second parts of Equation (22) and Equation (23) present an influence of external load. $l + l^*$ is the equivalent kink length [11]. l^* is the artificial parameter introduced for the case when the kink initiates and its length is infinitesimal ($1 \to 0$). In Equation (21) E_o is the Young's modulus of the virgin material.

The criterion (21) allows us to estimate the most favorable inclination of mesocracks ($\hat{N}_m$) as for kinks propagation and the fan of their inclination $\phi_{k1} < \phi_k < \phi_{k2}$. One can separate, as in Equations (19) and (20), the numbers of:

- opened mesocracks potent enough to kinks creation

$$\hat{N}_m^{(o)} = \frac{2(\phi_{k2}^{(o)} - \phi_{k1}^{(o)})}{\pi} N \tag{24}$$

and

- closed mesocracks

$$\hat{N}_m^{(c)} = \frac{2(\phi_{k2}^{(c)} - \phi_{k1}^{(c)})}{\pi} N \tag{25}$$

respectively. Obviously, the kink number is two times greater than $\hat{N}_m$.

When the "worst" kinked mesocrack becomes unstable, the final failure can take place with great probability. Its unconstrained propagation is very close to vertical direction, splitting prismatic specimen into parts.

2.5. Deformation Process for Unloading Path

We assume that in the two-dimensional stress state, the unloading process of the material starts when:

1. the stress components do not increase and
2. at least one of the two components σ_1, σ_2 decreases.

In general, the number of mesocracks

$$N_m = N_m^{(o)} + N_m^{(c)} = \text{constr.} \tag{26}$$

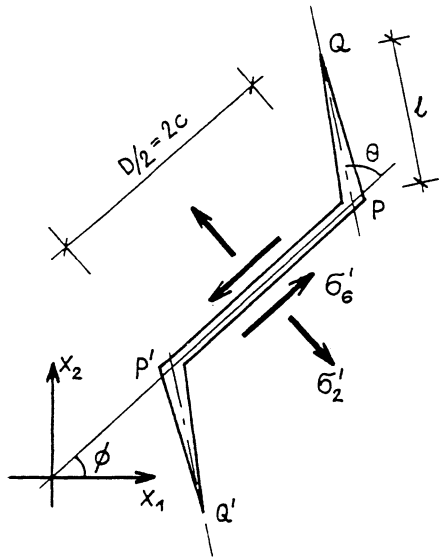

Figure 2. *Straight mesocrack PP′ with tension cracks P′Q′ and PQ.*

and the number of existing kinks

$$N_k = 2(\hat{N}_m^{(o)} + \hat{N}_m^{(c)}) = \text{constr.} \tag{27}$$

although, in particular cases of the current state $\underline{\sigma}$, small changes are possible. Further we postulate that during unloading:

1. The plastic strains do not change
2. The mesocracks can remain closed or opened in dependence on the local state of stress $\underline{\sigma}'$
3. Kinks of the mesocracks start to open, close or propagate in relation to $\underline{\sigma}'$

It is worth noticing that a small part of closed mesocracks can back-slide, when their surface roughness is not very high. In the after-mentioned numerical examples, this effect was not taken into account.

3. ILLUSTRATIVE EXAMPLES

3.1. Initial Data

Numerical calculations, showing the capability of the presented model, were performed for the following values of the basic MgO parameters (see e.g., References [1] and [12]):

- Young's modulus $E_o = 316.4$ GPa
- Poisson's coefficient $\nu_o = 0.272$
- Kirchhoff's modulus $G_o = 121.9$ GPa
- the surface energy of grains $\gamma_g = 1.0$ N/m
- the shear stress resistance for uniaxial compression $\tau_{so}^c = 75$ MP
- the shear stress resistance for uniaxial tension $\tau_{so}^t = 25$ MPa

In calculation we assume that surface energy of grain boundaries is $\gamma_{gb} = 0.5\ \gamma_g$ and the mean grain diameter in the unit cell is $\bar{D} = 45\ \mu$m. We simplify also that grains are hexagonal in shape ($\theta = 60°$).

3.2 Simple State of Stress

Let us apply the theoretical procedure of calculation: the compliance tensors $\underline{\underline{S}}$, $\underline{\underline{S}}^u$ and the damage tensor $\underline{\omega}$ (described in Reference [4]) to deformation process of MgO ceramic. First we consider the simple state of stress like: uniaxial tension, uniaxial compression and the two-dimensional—pure shear.

3.2.1 UNIAXIAL TENSION

In deformation process of uniaxial tension cracks propagate under mixed mode. We assume that newly initiated microcracks spread immediately to the whole facet of grain. Consequently, we have only opened mesocracks within the unit cell ($N_m^{(o)} > 0$; $N_m^{(c)} = 0$). A typical diagram for constitutive relation is presented in Figure 3. It has characteristic shape with the local inflection, as in the case of pure brittle solids [13,14], when mesocrack density is achieved. Segment 0–1 reflects purely linear elastic response of the MgO ceramic. At point 1 the first conjugate slip systems are created inside the grains. They are potent enough to nucleate the first mesocrack at point 2. Segment 2–3 represents the nucleation and development of mesocracks. At point 3 the saturation state is reached and the "worst" mesocrack is able to kink and spread along grain boundaries causing final failure. It is worth pointing out that there is no continuity in 2 as for tangent, like in References [13] and [14], due to the fact of intensive mesocrack initiation at the beginning of fissuration process. As an illustration, Figure 4 shows changes of the mesocrack number for the unit cell containing 200 grains. Its character is similar to that which was proposed for Al_2O_3 in References [13] and [14]. Although the increase tendency for the state preceding the final failure is kept, the less preferential mesocracks inclination to the tension direction causes lowest influence on the total mechanical response of the material.

Variation of the unloading modulus S_{11}^u is depicted in Figure 5. Its shape results from the assumption that just after nucleation process microcracks become mesocracks. Consequently, S_{11}^u decreases more at the beginning of fissuration and is approximately 21% less in comparison to S_{11}^o before the final failure.

Figure 6 shows distribution of the damage component ω_1 following Equation

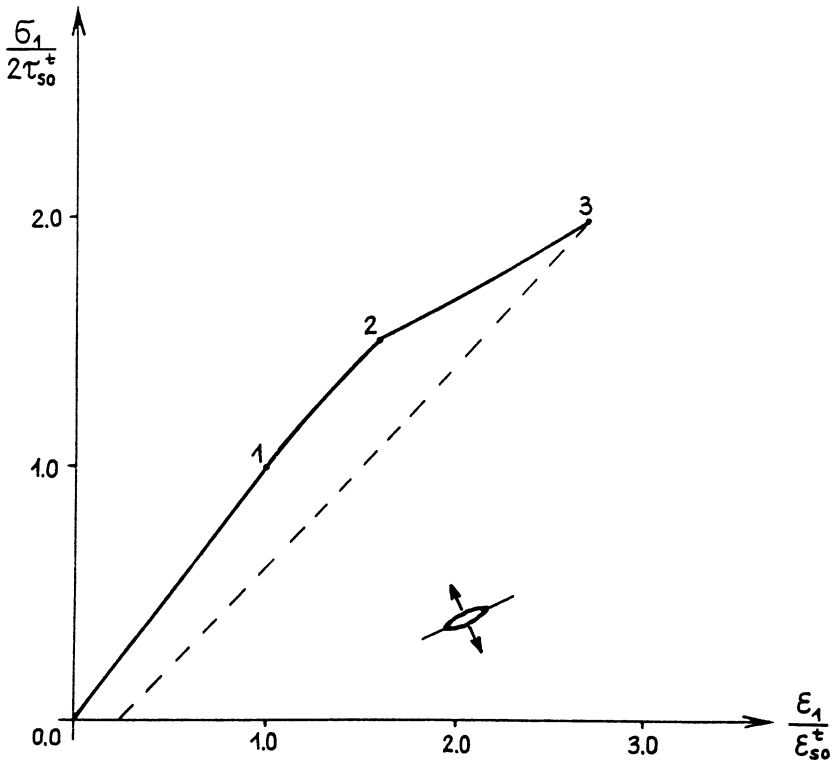

Figure 3. *Stress-strain relation for uniaxial tension.*

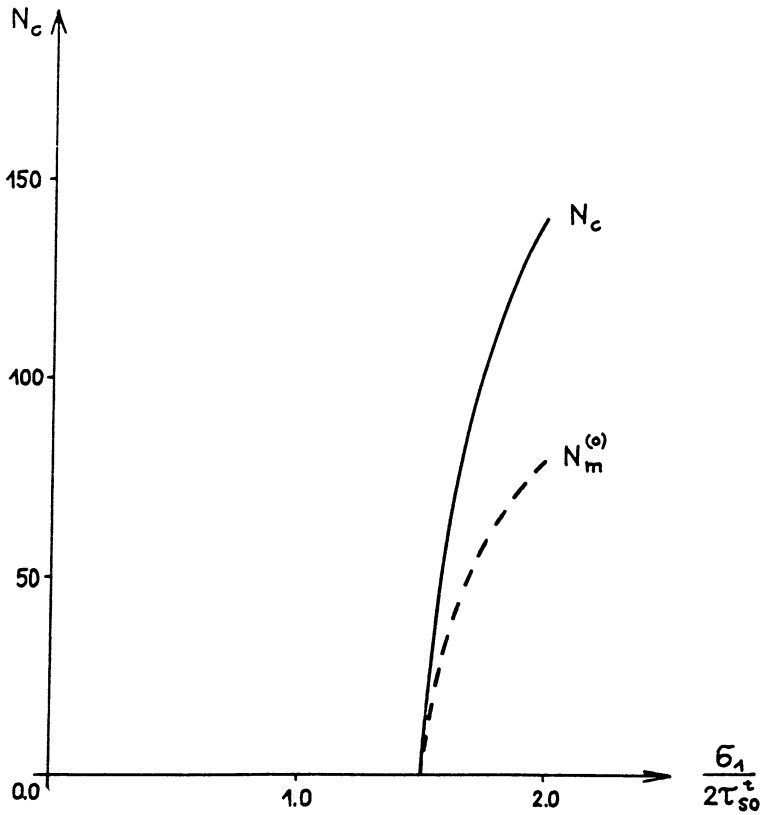

Figure 4. *Numbers of the initiated cracks and mesocracks inside the unit cell.*

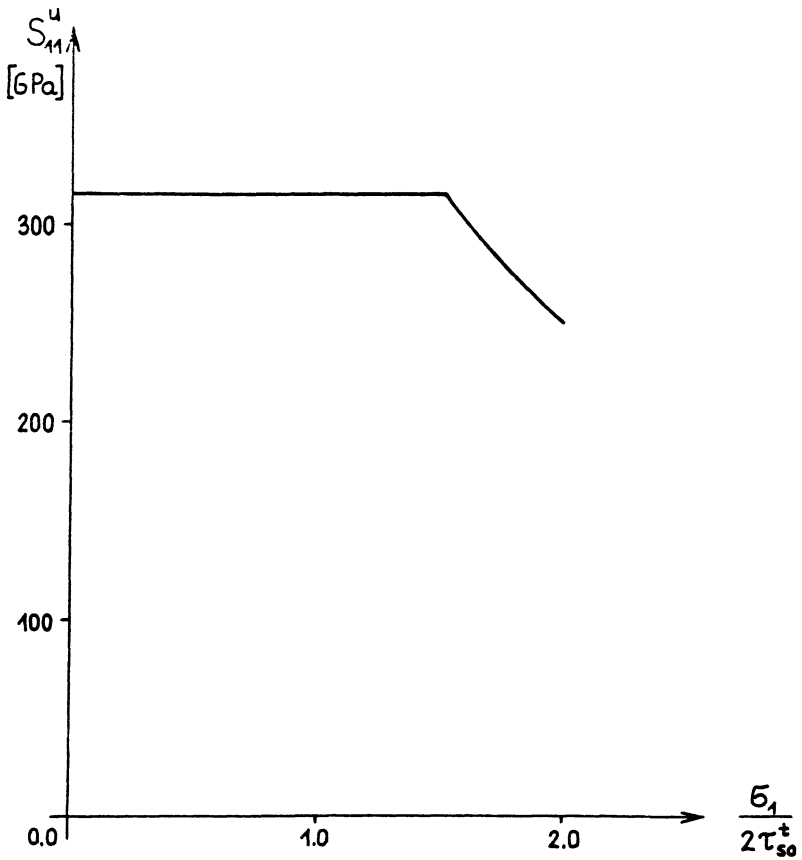

Figure 5. *Distribution of the unloading compliance* S^u_{11}.

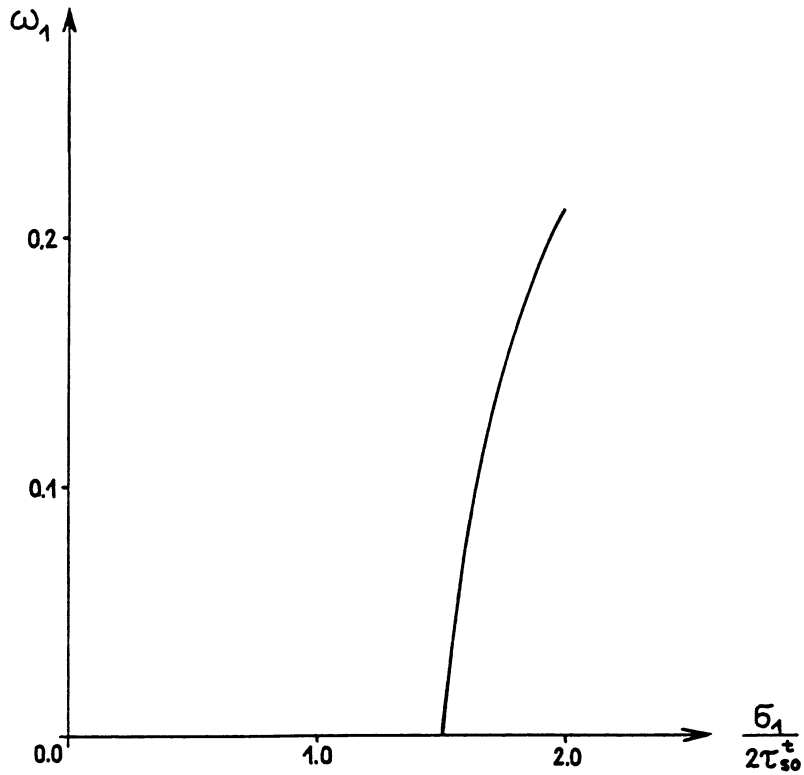

Figure 6. *Distribution of the damage component* ω_1.

(6) with assumption that all cracks close ideally. The theoretical derivations lead to the conclusion that $\omega_2 = 0$, because fissuration process under tension does not create strain increase in direction 2. One can conclude that the assumption ν = constant, postulated in damage models formulated on the basis of "strain equivalence hypothesis," [15], is reasonable for materials with distributed straight slits.

3.2.2 PURE SHEAR

During deformation process under shear we have both tension and compression mesocracks within the unit cell ($N_m^{(o)} > 0$; $N_m^{(c)} > 0$). It was assumed in numerical calculations that friction sliding coefficient $\mu = 0.3$. Figure 7 presents correlation $\sigma_2(\epsilon_2)$, whereas Figure 8 shows $\sigma_1(\epsilon_1)$, respectively. Segment 0–1 reflects purely linear elastic response. At point 1 the first conjugate slip systems are created inside the grains. They are potent enough to produce the first mesocrack at point 2. Segment 2–3 represents the nucleation and development of

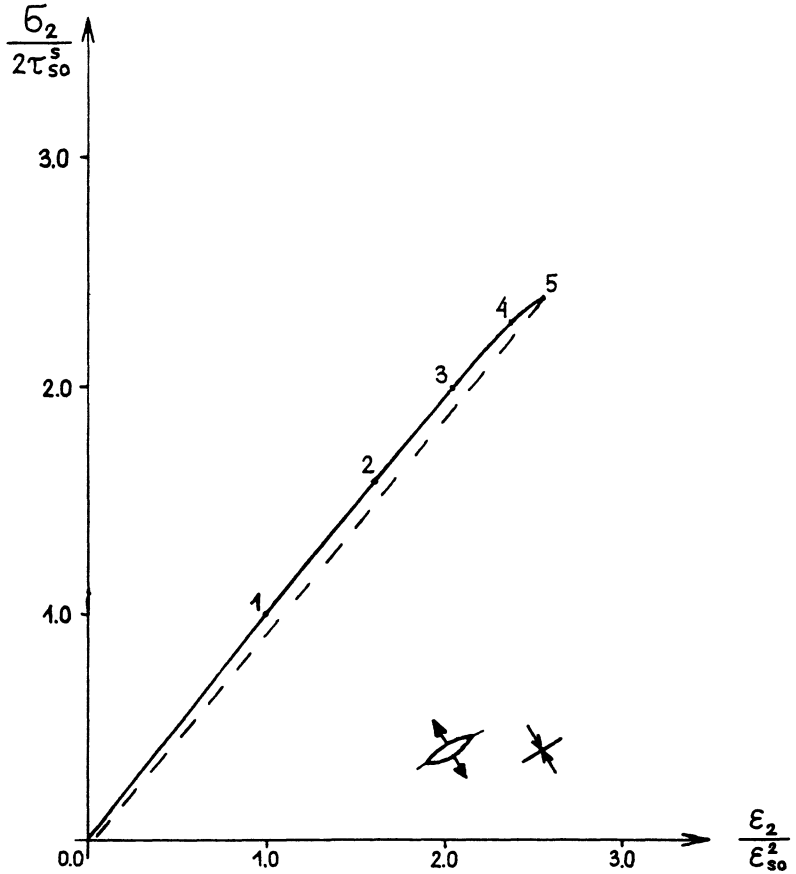

Figure 7. *Stress-strain relation $\sigma_2(\epsilon_2)$ for pure shear.*

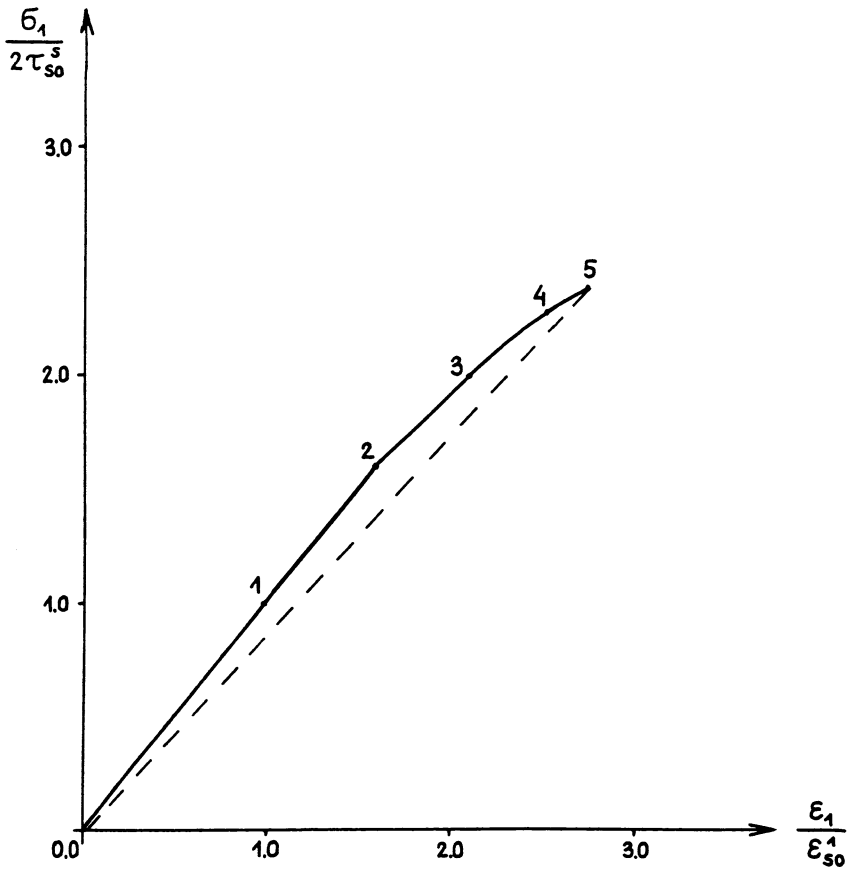

Figure 8. *Stress-strain relation $\sigma_1(\epsilon_1)$ for pure shear.*

mesocracks. As in uniaxial tension function, $\sigma_1(\epsilon_1)$ has the characteristic shape with the small inflection, whereas $\sigma_2(\epsilon_2)$ is smooth. At point 3 the first opened mesocrack kinks and spreads under stable manner. The first compressed mesocrack changes its direction at the load level corresponding to point 4. Final failure is associated with unstable unconstrained propagation of compressed mesocracks.

Figure 9 presents the evolution of all kinds of defects appearing inside the unit cell. Its distribution is similar to that of Figure 4.

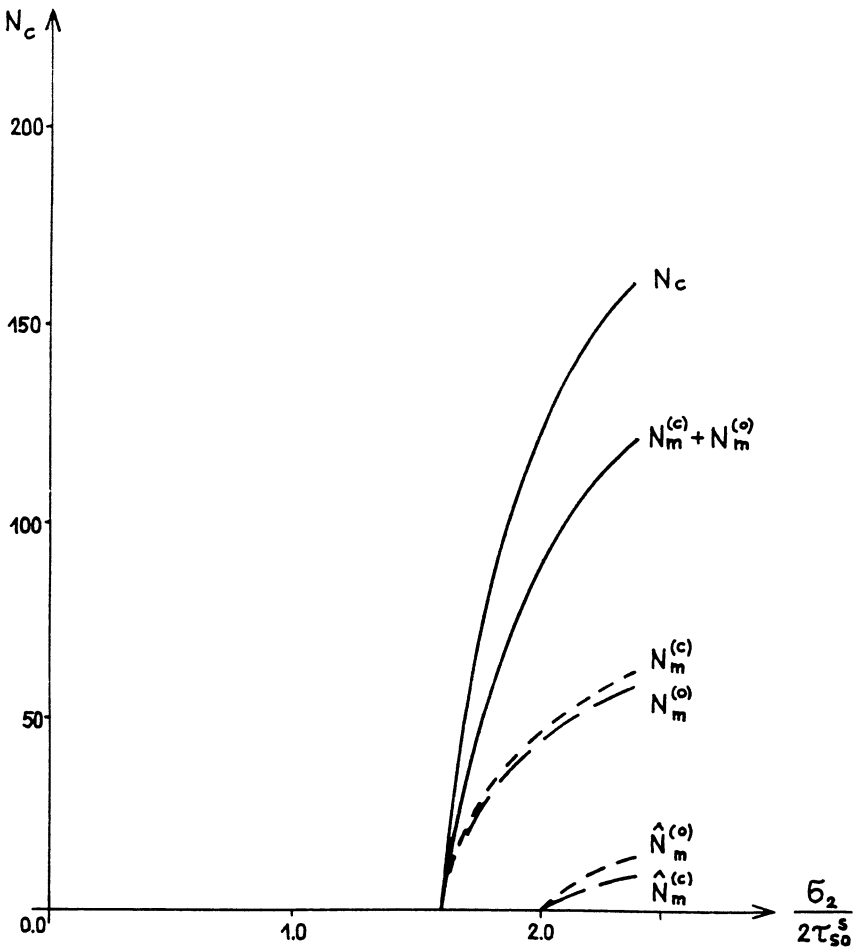

Figure 9. *Numbers of the initated cracks, the mesocracks and kinked mesocracks inside the unit cell for pure shear.*

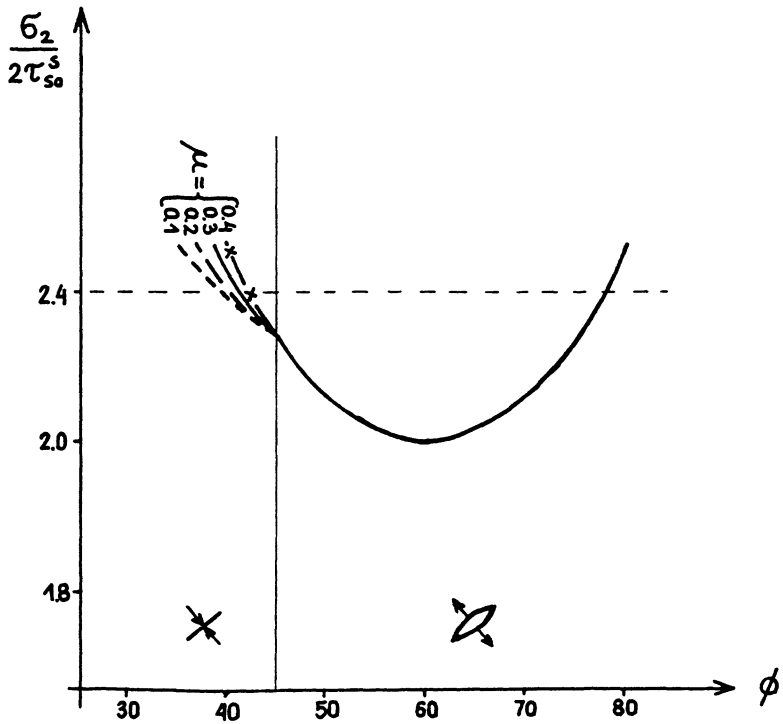

Figure 10. *Ability of the mesocracks to kinking process.*

One can get more detailed information about ability of mesocracks to kinking from Figure 10. Although most of opened mesocracks $N_m^{(o)}$ can create tensil cracks, only a small part of them ($65° < \phi < 73°$) are subjected to external loading which permits their stable development. Closed mesocracks are inclined in the very narrow region but all of them can spread quicker than opened ones, leading to failure of the material. The calculations were performed for different values of friction sliding coefficient μ.

Changes of the unloading compliance tensor S^*_{22} and S^*_{11} are depicted in Figure 11. The closed mesocracks play a very important role in the unloading process. The difference between starred and unstarred curves shows their influence on the unloading material response. Namely, the starred lines are estimated assuming no backsliding of the mesocracks, whereas unstarred lines are associated with their total backsliding. Maximal reduction of S^*_{22} and S^*_{11} in the case of no backsliding equals 1% and 9%, whereas for total backsliding 5% and 13% appropriately.

The state of damage ω_2 and ω_1 is strictly connected with the unloading compliance tensor $\underline{S}^*$ (see Figure 12). The influence of the mesocracks' backsliding is

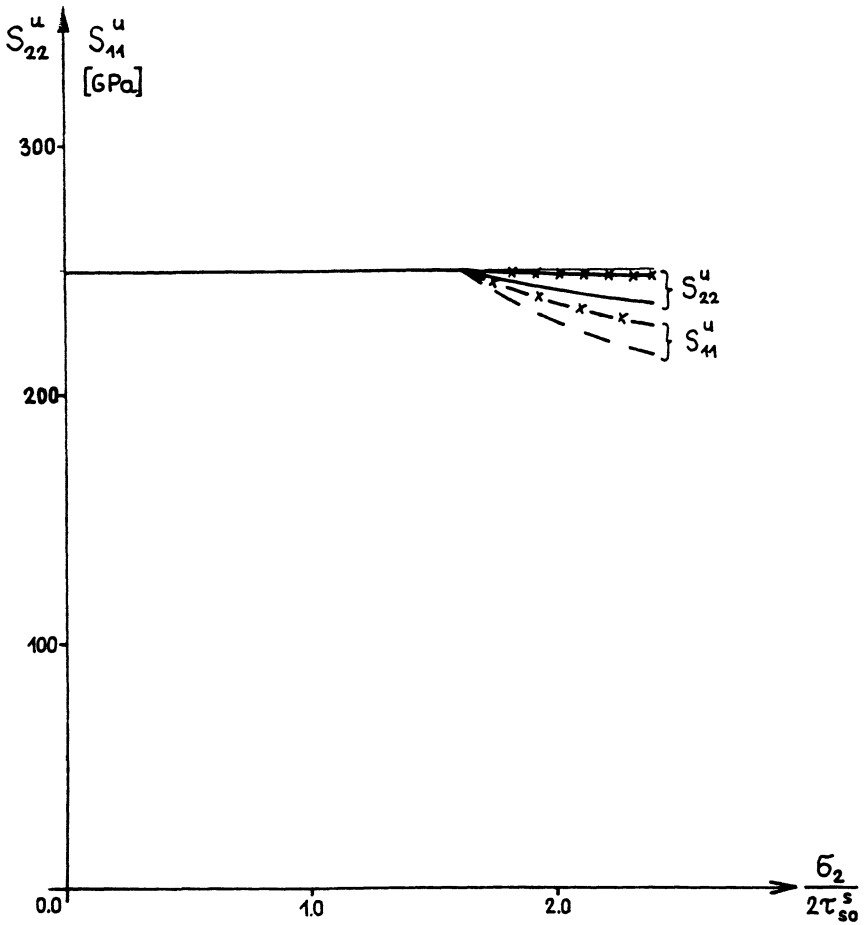

Figure 11. *Distributions of the unloading compliances* S_{22}^u *and* S_{11}^u.

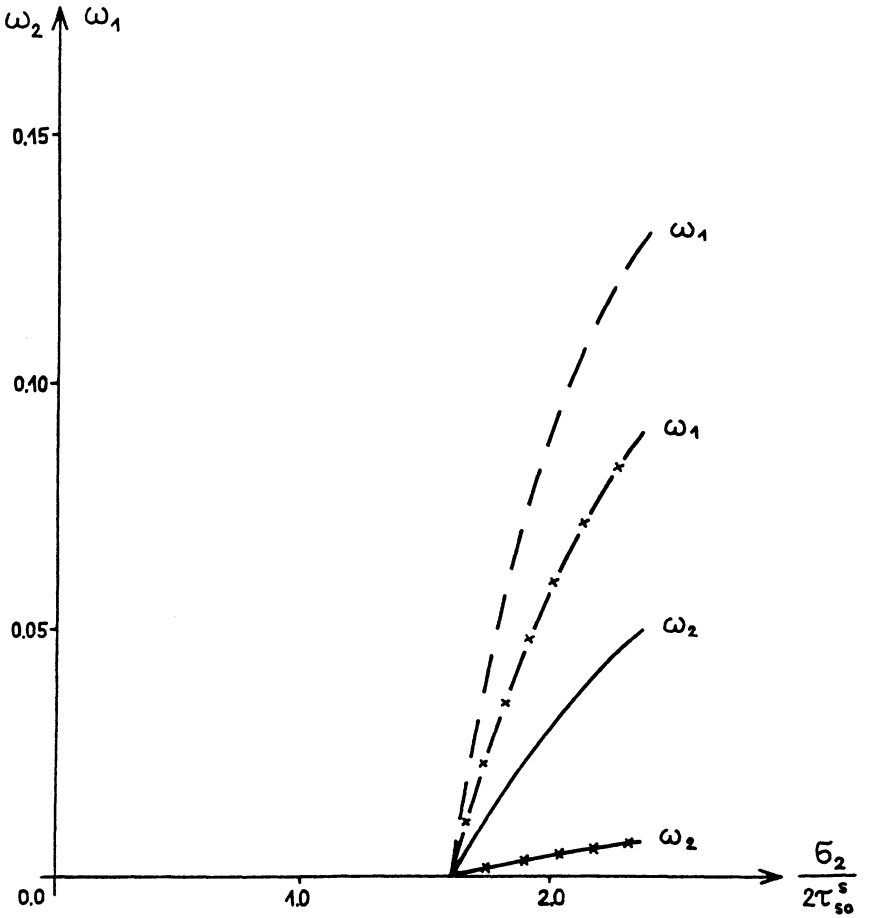

Figure 12. *Distributions of the damage components* ω_2 and ω_1.

much higher on the damage in direction 2. The damage component in direction 1 is much greater in comparison to ω_2. It means that the component ω_1 is dominant mode of the material degradation and the specimen failures by splitting along direction 2.

3.2.3 UNIAXIAL COMPRESSION

The detailed description of deformation under uniaxial compression was presented in Reference [4]. We will quote the most important results for completeness of the present paper.

Contrary to the previous paragraphs, under compression of the material only closed mesocracks appear ($N_m^{(o)} = 0$; $N_m^{(c)} > 0$). As in §3.2.2. numerical calculations were performed for $\mu = 0.3$.

Figure 13 presents a typical distribution of the function $\sigma_2(\epsilon_2)$. Segment 0–1 reflects purely linear elastic response of the material. At point 1 the slip line phase initiates. Nucleation of Zener-Stroh's microcracks begin in point 2. Segment 2–3 obeys nucleation and development of mesocracks. The frictional sliding of some suitably oriented mesocracks initiates tension cracks at their ends. Further loading (3–4) causes growth of the tension cracks and spreading along the sequent segment of grains. At point 4 some tension cracks are able to kink again or spread through an adjacent crystal [Figure 1(f)].

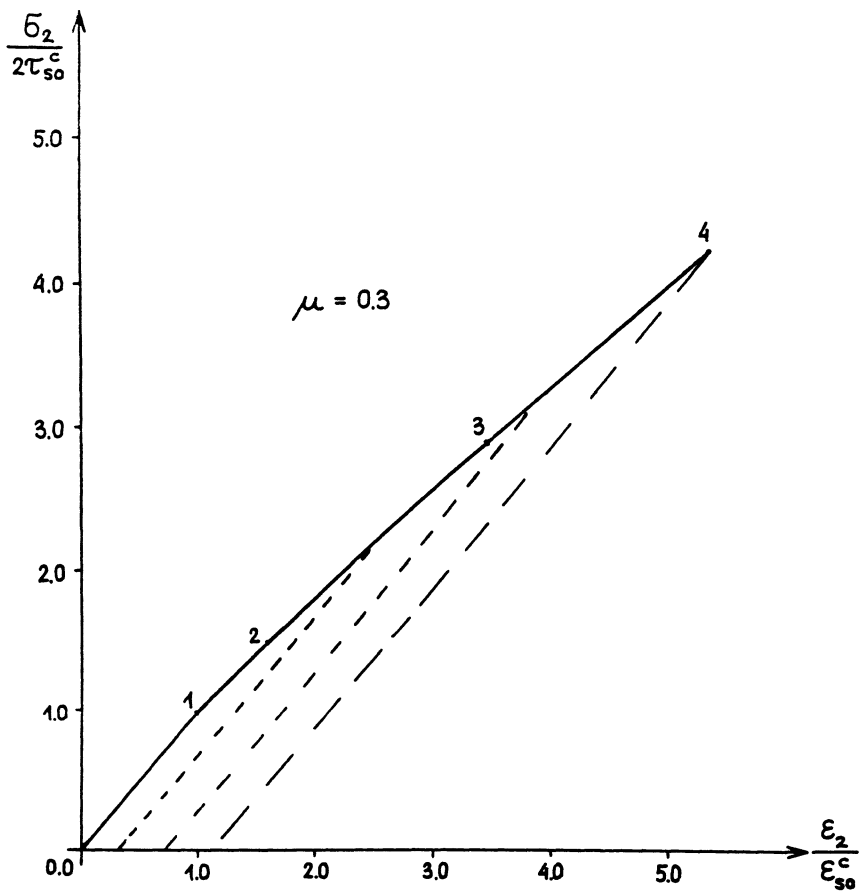

Figure 13. *Stress-strain relation $\sigma_2(\epsilon_2)$ for uniaxial compression.*

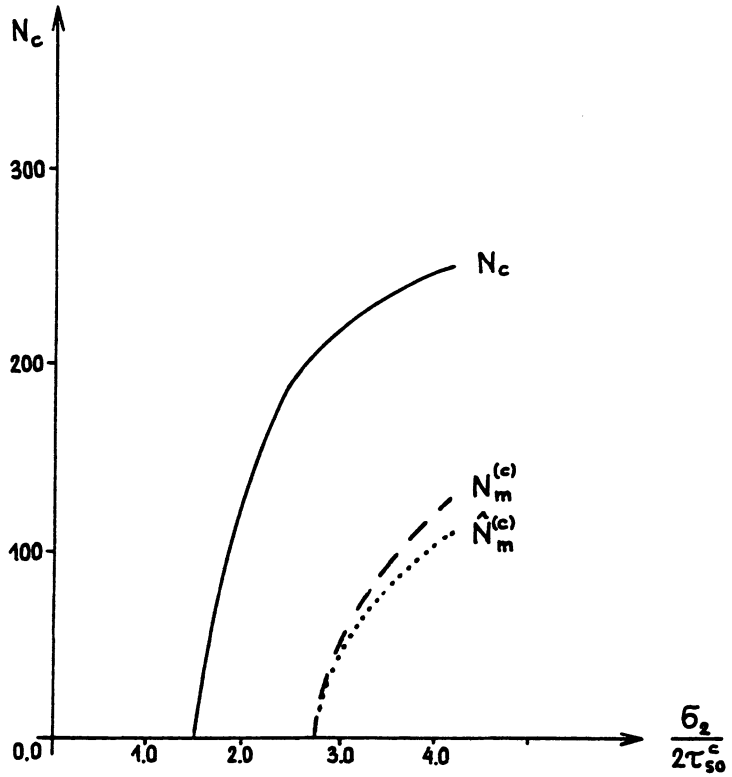

Figure 14. *Numbers of the initiated cracks, the mesocracks and kinked mesocracks inside the unit cell.*

Figure 14 shows increase of all defect numbers inside the unit cell. As in previous examples these increases are the most intensive for all types of defects at the beginning. It is worth noting that the first kink appears almost parallel to the creation of the first mesocrack.

Variation of the unloading compliance S^u_{22} is plotted in Figure 15. The starred line was estimated for the case of no backsliding of mesocracks. In the final state S^u_{22} is about 1% less in comparison to S^u_{22}. The continuous line presents the case of total backsliding of mesocracks. S^u_{22} is about 3% less in comparison to S^u_{22}.

The damage state $\underline{\omega}$ presents Figure 16. It is interesting to point out that for uniaxial compression the shape of curves is more closed to expected one. It is caused by the fact that in uniaxial compression crack propagation process obeys all states—from nucleation to the secondary kinking. It allows more detailed description of the whole material degradation. Obviously the material damage is much higher in direction 1 and specimen failure by splitting along direction 2.

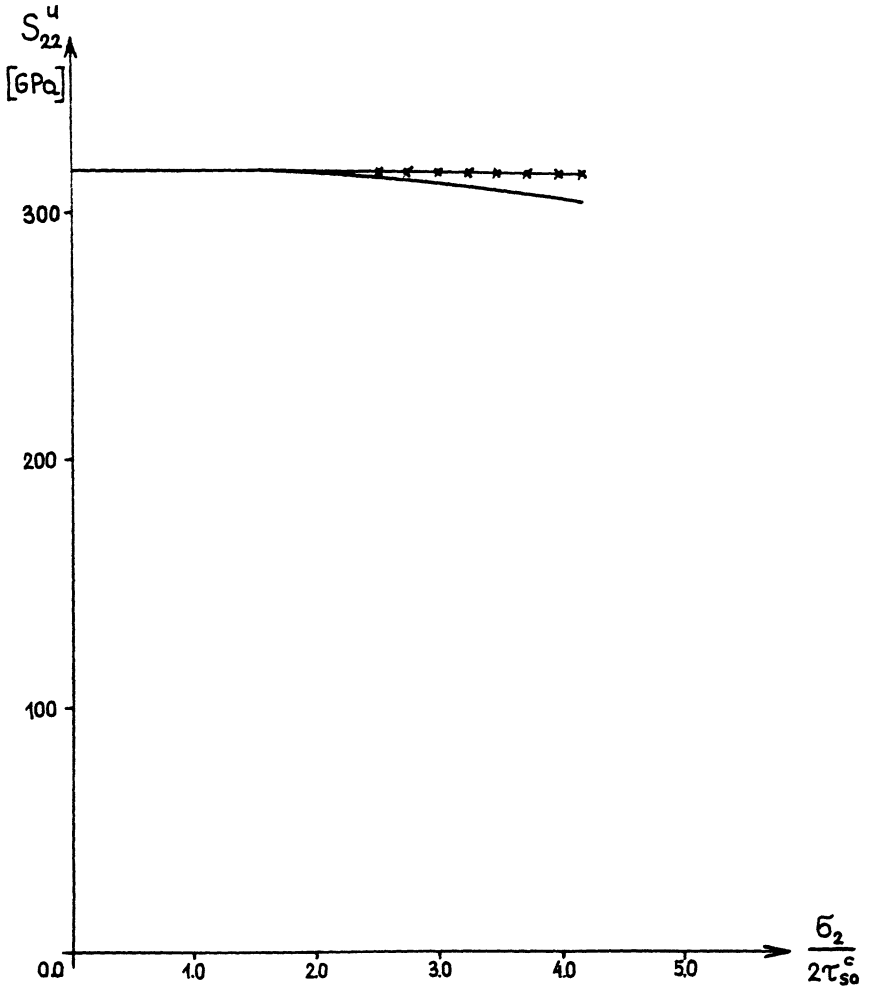

Figure 15. *Distribution of the unloading compliance* S_{22}^{u}.

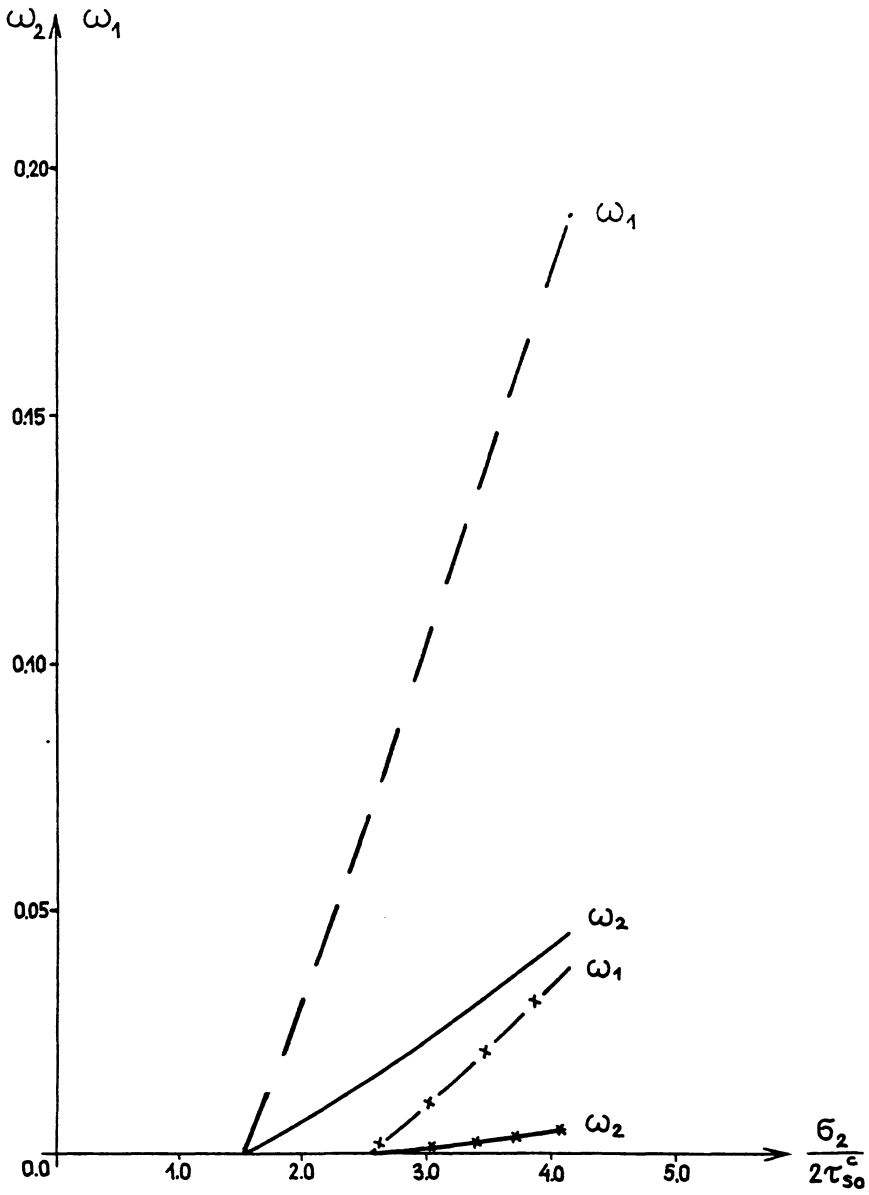

Figure 16. *Distribution of the damage components ω_2 and ω_1.*

3.3. Limit Surfaces for Two-Dimensional Tension-Compression

The more detailed numerical calculations for different values of the coefficient $k \langle -\infty, 0 \rangle$ characterizing external loading, according to Equation (10), allow to plot several limit surfaces appearing during whole deformation process. Figure 17 shows four characteristic threshold lines. The first one describes slip line initiation phase. Having experimental data for uniaxial tension and compression only, we assume linear shape of this surface. The second one concerns the first mesocracks' initiation during deformation process. The third one is connected with kink initiation mechanisms and overlaps with the last one, the final failure envelope, from uniaxial tension to pure shear state. When $k < -1$ these two surfaces differ markedly.

The region tension-tension state of stress was not investigated numerically and is only approached by straight lines.

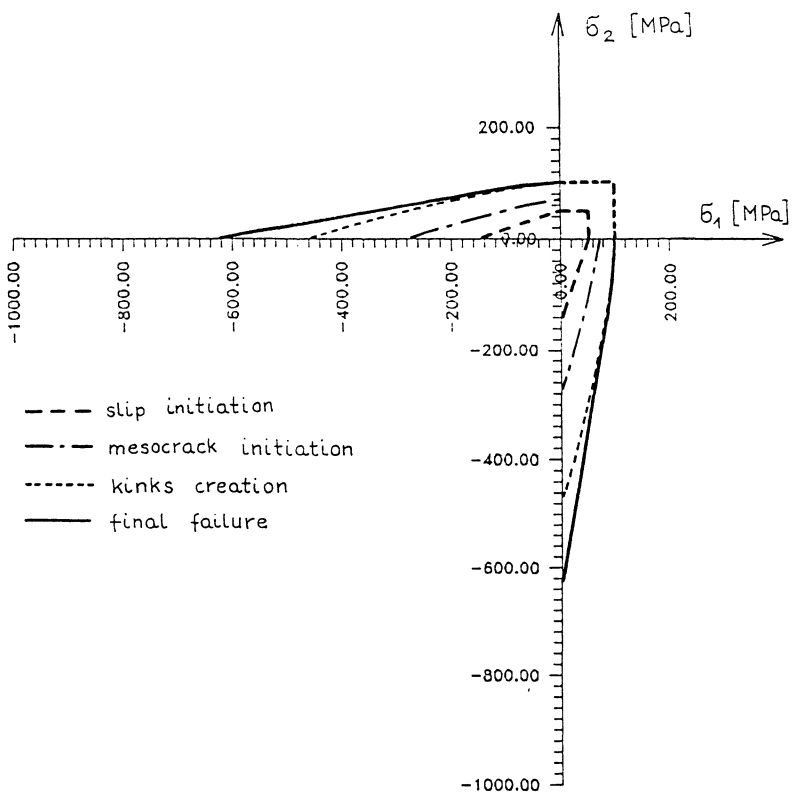

Figure 17. *Limit surfaces for the two-dimensional stress state.*

Concluding, the slightly nonlinear final failure limit curve can be approximated for engineering applications by the Coulomb-Mohr condition. It was done in the crashing process analysis of ceramic cylinder subjected to uniaxial compression [16].

4. FINAL REMARKS

The deformation process of semi-brittle materials obeys many different phenomena developing within the material. Most of them are taken into account. In this way the model does not require introduction of any material parameter both for loading and unloading process. The most important thing is possibility of estimation, on the basis of the physics, damage parameters (by unloading compliance tensor) appearing in many phenomenological models describing internal degradation. Obtained results lead to conclusion that damage low (2), for engineering applications, can be postulated in the form very close to linear in relation to stress. However, in the stages preceding the final failure, where cracks spread in unconstrained manner [17] and interaction effects play an important role, presented model should be appropriately modified [7].

ACKNOWLEDGEMENT

The author gratefully acknowledges the financial support rendered by the research grants from:

- the German Research Society's (DFG), Project No. 218/1-2 on dynamic testing of high strength ceramics and
- the Research Committee, Poland, KBN Project No. 3 1014 91 01 on thermomechanics of damage development and phase transformation in materials

REFERENCES

1. Davidge, W. 1979. *Mechanical Behaviour of Ceramics,* Cambridge, U.K.: Cambridge University Press.
2. Stokes, R. J. 1972. "Microscopic Aspects of Fracture in Ceramics," in: *Fracture* Vol. VII, H. Liebovitz ed., New York: Academic Press, pp. 157–241.
3. Papadopoulos, G. A., V. N. Kyptopoulos and T. Sandowski. 1994. "Experimental Study of Fracture Process in MgO Polycrystalline Ceramics," *The Fourth International Symposium on Brittle Matrix Composites,* Cambridge-Warsaw: Woodhead Publ., pp. 634–643.
4. Sadowski, T. 1994. "Mechanical Response of Semi-Brittle Ceramics Subjected to Tension-Compression State. Part I: Theoretical Modelling," *Int. J. Dam. Mech.*, 3:212–233.
5. Sadowski, T. 1994. "Modelling of Semi-Brittle MgO Ceramic Behaviour under Compression State," *Mech. Mater.*, 18:1–16.
6. Sadowski, T. 1995. "Stress Induced Anisotropy of Semi-Brittle Polycrystalline Materials under Simple Shear," *Arch. Mech.* (submitted).
7. Sadowski, T. 1995. "General Formulation of the Constitutive Relations for Semi-Brittle Materials," *Acta. Mech.* (submitted).

8. Smith, E. and J. Barnby. 1967. "Crack Nucleation in Crystalline Solids," *Metal Sci. Jour.*, 1:56–66.
9. Krajcinovic, D. and A. Stoimirovic. 1990. "Deformation Process in Semibrittle Polycrystalline Ceramics," *Int. J. Fracture*, 42:73–85.
10. Stoimirovic A., D. Krajcinovic and T. Sadowski. 1987. "Constitutive Model for Polycrystalline MgO Ceramics," in *Constitutive Modelling for Nontraditional Materials*, V. Stokes and D. Krajcinovic, eds., *ASME Publ., AMD*–Vol. 85:175–187.
11. Horii, H. and S. Nemat-Nasser. 1986. "Brittle Failure in Compression: Splitting, Faulting and Brittle-Ductile Transition," *Phil. Trans. R. Soc. Lond.*, A, 319:337–374.
12. Gilmann, J. J. 1961. "Mechanical Behavior of Ionic Crystals," in *Progress in Ceramic Science*, J. E. Burke, ed., New York: Pergamon Press, Vol. 1, pp. 146–212.
13. Fu, Y. and A. G. Evans. 1985. "Some Effects of Microcracks on the Mechanical Properties of Brittle Solids–I. Stress, Strain Relations," *Acta Metall.*, 33:1515–1523.
14. Evans, A. G. and Y. Fu. 1985. "Some Effects of Microcracks on the Mechanical Properties of Brittle Solids–II. Microcrack Toughening," *Acta Metall.*, 33:1523–1531.
15. Lemaitre, J. 1985. "A Continuous Damage Mechanics Model for Ductile Fracture," *Trans. ASME, J. Eng. Mat. Tech.*, 107:83–89.
16. Sadowski, T. and Z. Mróz. 1991. "Deformation Process of Low MgO Ceramic Cylinder under Compression State," in *The Third International Symposium on Brittle Matrix Composites*, London, New York: Elsevier, pp. 366–375.
17. Ritter, J. E. 1992. "Crack Propagation in Ceramics," in *Engineered Materials Handbook*, Vol. 4: Ceramics and Glass, *ASME International*, pp. 694–705.